

# Nanoscaled Sn and Pb Particles Aligned in Al<sub>2</sub>O<sub>3</sub> Tubes Obtained from Molecular Precursors

Michael Veith,<sup>\*[a]</sup> Jacqueline Frères,<sup>[a]</sup> Peter König,<sup>[a]</sup> Oliver Schütt,<sup>[a]</sup> Volker Huch,<sup>[a]</sup> and Joel Blin<sup>[a]</sup>

**Keywords:** Tin and lead clusters / Nanoparticles / Al<sub>2</sub>O<sub>3</sub> tubes / Alignment of metal clusters / Alkoxy- and siloxyaluminum amides

Tin and lead nanoparticles and metal sponges were prepared by reducing Me<sub>2</sub>Si(NtBu)<sub>2</sub>Sn (**7**) and Me<sub>2</sub>Si(NtBu)<sub>2</sub>Pb (**9**) with [H<sub>2</sub>AlOtBu] (**3**), [HAl(OtBu)<sub>2</sub>] (**13**), [H<sub>2</sub>AlOSiMe<sub>2</sub>tBu] (**8**), and [(Me<sub>2</sub>tBuSiO)<sub>2</sub>AlH] (**15**). Together with dihydrogen and the metals in their elemental state the monomeric compounds [Me<sub>2</sub>Si(NtBu)<sub>2</sub>Al(OSiMe<sub>2</sub>tBu)(THF)] (**10**) and [Me<sub>2</sub>-Si(NtBu)<sub>2</sub>Al(OtBu)(THF)] (**11**) can be obtained, to mention only two examples. Each monomer is stabilized by a THF molecule coordinated to aluminum, which on sublimation loses its donor molecule and dimerizes through Lewis acid-base interactions to the spiro compounds [Me<sub>2</sub>Si(NtBu)<sub>2</sub>AlO-SiMe<sub>2</sub>tBu]<sub>2</sub> (**12**) and [Me<sub>2</sub>Si(NtBu)<sub>2</sub>AlOtBu]<sub>2</sub> (**4**), respectively. The molecular structures of **10**, **11**, and **12** were determined by single-crystal X-ray diffraction techniques. The reduction of **7** at -115 °C is gradually indicated by a color change of the reaction mixtures from red to dark brown with increasing temperature and depending on the reducing agent used. The tin powders that were obtained were identified as β-tin using X-ray powder diffraction techniques and their average crys-

tallite size depends on the polarity of the solvent and hydride used. Under certain conditions metal sponges are formed. Pycnometric measurements were carried out on the tin and lead sponges. These showed almost the known densities for the metals when helium was used whereas significantly smaller ones were measured in water. Porous alumina membranes of different pore diameters were filled with tin and lead particles. Metal nanoparticles were prepared within the tubes of the membranes by reduction of the metal amides in the pores. The infiltration process can be repeated up to ten times increasing the amount of particles within the tubes monitored by SEM. The obtained brown or black membranes were characterized by SEM, EDX, and UV/Vis analysis. The filled membranes show sharp impervious ranges in the UV/Vis spectrum between 270 and 525 nm and could therefore be used as wavelength filters.

(© Wiley-VCH Verlag GmbH & Co. KGaA, 69451 Weinheim, Germany, 2005)

## Introduction

During the last years metal clusters and colloids have become more and more important as building blocks in the synthesis of organized nanostructured materials. Because of the various applications of metal nanoparticles many articles have emerged, especially in the field of surface-enhanced spectroscopy or photocatalysis. In addition, studies on the size-controlled synthesis and the self-assembly of clusters have appeared.<sup>[1,2]</sup> Interestingly, the majority of the publications deal with the synthesis and the properties of transition or noble metal nanoparticles,<sup>[3]</sup> whereas comparatively little is known about colloidal nanoparticles of main group metals.<sup>[4]</sup>

In this work we describe the preparation of tin and lead colloids and clusters on the nanometer scale using chemical control. The syntheses are based on an organometallic route, which we have already described in former reports.<sup>[5,6]</sup> In this route, tin and lead amides are reduced by

siloxo- or alkoxyalanes in organic solvents leading to tin or lead particles, together with dihydrogen and siloxo or alkoxy compounds. A proposal for the mechanism of the formation of the aluminum compounds is given in this report. By controlling different parameters, e.g. temperature and concentration of the starting materials, it was possible to obtain tin and lead particles either stabilized as colloids or as metal powders and sponges.

We have been able to insert the metal particles into porous alumina membranes of different pore diameters. The membranes were produced for our use by G. Schmid et al., who have already used such membranes for one-dimensional ordering of gold colloids.<sup>[7]</sup>

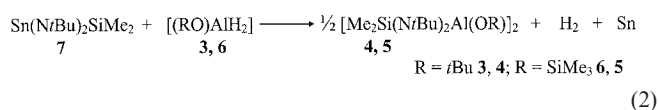
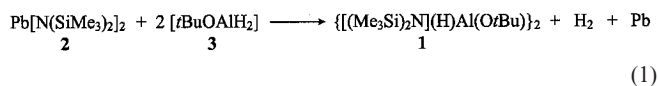
## Results and Discussion

### Syntheses and Reaction Mechanism

Tin and lead particles can be efficiently obtained by reduction of tin or lead amides with siloxo- or alkoxyalanes in organic solvents. Besides dihydrogen, a siloxo- or an alkoxyaluminum amide is formed through ligand exchange.

[a] Institut für anorganische Chemie, Universität des Saarlandes, Postfach 151150, 66041 Saarbrücken, Germany  
E-mail: veith@mx.uni-saarland.de

In former publications we reported on the formation of the alkoxy(amino)alane [(Me<sub>3</sub>Si)<sub>2</sub>N(H)Al(O*t*Bu)] (**1**) in a redox reaction between the lead amide Pb[N(SiMe<sub>3</sub>)<sub>2</sub>]<sub>2</sub> (**2**)<sup>[8]</sup> and a double equivalent of the *tert*-butoxyalane [H<sub>2</sub>Al(O*t*Bu)] (**3**)<sup>[9]</sup> [Equation (1)].<sup>[6]</sup> The spirocyclic compounds [Me<sub>2</sub>Si(N*t*Bu)<sub>2</sub>Al(O*t*Bu)]<sub>2</sub> (**4**) and [Me<sub>2</sub>Si(N*t*Bu)<sub>2</sub>AlOSiMe<sub>3</sub>]<sub>2</sub> (**5**) have been obtained by stoichiometric reactions of [H<sub>2</sub>Al(O*t*Bu)] (**3**) or [H<sub>2</sub>AlOSiMe<sub>3</sub>] (**6**),<sup>[10]</sup> respectively, with the cyclic diazastannylene Me<sub>2</sub>Si(N*t*Bu)<sub>2</sub>Sn (**7**)<sup>[11]</sup> [Equation (2)].<sup>[5]</sup>



Using a similar procedure we have recently treated the stannylene Me<sub>2</sub>Si(N*t*Bu)<sub>2</sub>Sn (**7**) with [H<sub>2</sub>Al(OSiMe<sub>2</sub>*t*Bu)] (**8**) and the plumbylene Me<sub>2</sub>Si(N*t*Bu)<sub>2</sub>Pb (**9**) with [H<sub>2</sub>Al(O*t*Bu)] (**3**) in equimolar ratios [Equations (3)–(5)]. We were able to isolate the monomeric compounds [Me<sub>2</sub>Si(N*t*Bu)<sub>2</sub>Al(OSiMe<sub>2</sub>*t*Bu)(THF)] (**10**) and [Me<sub>2</sub>Si(N*t*Bu)<sub>2</sub>Al(O*t*Bu)(THF)] (**11**), each monomer being stabilized by a donor solvent molecule [Equation (3)]. If the compounds **10** and **11** are sublimed, they release the solvent donors and dimerize to the spiro compounds [Me<sub>2</sub>Si(N*t*Bu)<sub>2</sub>Al(OSiMe<sub>2</sub>*t*Bu)]<sub>2</sub> (**12**) or to **4** [Equation (4)]. Both spirocyclic compounds can also be prepared in solution by heating the reaction mixtures [Equation (4)]. The monomeric compounds **10** and **11** have until now not been observed, and as in our

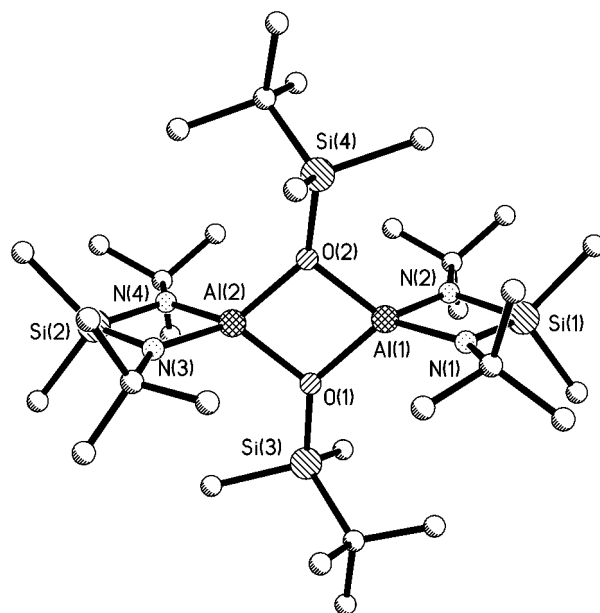
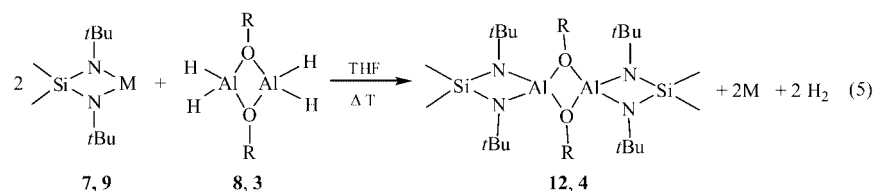
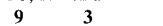
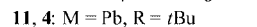
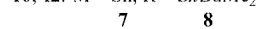
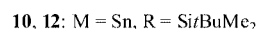
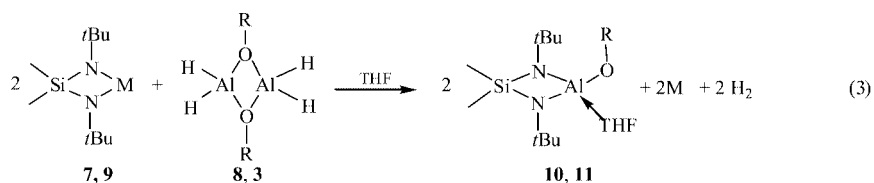


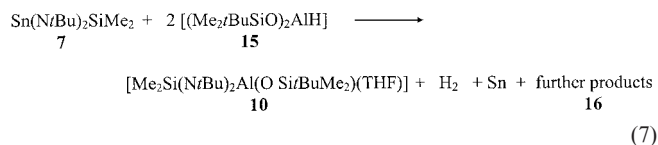
Figure 1. Selected bond lengths [Å] and angles [°] of **12**: Si(1)–N(1)/N(2) 1.746/1.742, Al(1)–N(1)/N(2) 1.838/1.827, Si(2)–N(3)/N(4) 1.746/1.744, Al(2)–N(3)/N(4) 1.832/1.834, Al(1)–O(1) 1.869, Al(1)–O(2) 1.879, Al(2)–O(1) 1.822, Al(2)–O(2) 1.876, O(1)–Si(3) 1.718, O(2)–Si(4) 1.713, N(1)–Si(1)–N(2) 90.89, N(1)–Al(1)–N(2) 85.43, Al(1)–N(1)–Si(1) 91.65, Al(1)–N(2)–Si(1) 92.09, N(3)–Si(2)–N(4) 91.01, N(3)–Al(2)–N(4) 85.59, Al(2)–N(3)–Si(2) 91.65, Al(2)–N(4)–Si(2) 91.65, Al(1)–O(1)–Al(2) 97.54, Al(1)–O(2)–Al(2) 97.42, O(1)–Al(1)–O(2) 82.65, O(1)–Al(2)–O(2) 82.37.

former workup the crude products were directly sublimed [Equation (5)].

The molecular structure of compound **12** (Figure 1) in the crystal is very similar to those of compounds **4** and **5**.<sup>[5]</sup> Selected bond lengths and angles are given in the caption of Figure 1 and are found within the expected ranges.







### Materials Part

By using our reduction procedure of the tin and lead amides it is possible either to stabilize the tin and lead particles as colloids in solution or to obtain them as nano-scaled powders or metal sponges depending on the chosen reaction conditions (temperature or concentration of the starting materials). With regard to the lead formation we have already reported in detail on the different species that may be produced.<sup>[6]</sup> Here we mainly want to discuss our results from the reduction of the tin compounds.

The polarity of the solvents used has an important influence on the diameters of the tin crystallites that are produced. We studied the reactions of **7** with **3** or **6** [see Equation (2)] in different polar solvents or solvent mixtures, respectively (see Table 1).

Table 1. Average crystallite sizes from analysis of peaks in X-ray powder diffraction data. Reaction of  $\text{Me}_2\text{Si}(\text{NtBu})_2\text{Sn}$  (**7**) with  $[\text{H}_2\text{AlOtBu}]$  (**3**) (a), or with  $[\text{H}_2\text{AlOSiMe}_3]$  (**6**) (b).

(a) Medium	Average crystallite size	(b) Medium	Average crystallite size
THF	<20 nm	THF	20–30 nm
THF/thiophene (10%)	60–80 nm	THF/thiophene (10%)	60–80 nm
THF/TMEDA (10%)	160–180 nm	THF/TMEDA (10%)	200–220 nm
Toluene	500–520 nm	Toluene	800–820 nm

When the reaction is started at  $-115\text{ }^\circ\text{C}$  (ethanol/liquid  $\text{N}_2$ ) a clear yellow solution forms. By warming the reaction mixture to room temperature a dramatic color change from red to dark brown takes place. On further heating the mixtures above  $40\text{ }^\circ\text{C}$ , black suspensions are formed. Obviously, the tin particles are in the first instance formed in a colloidal form (clear intensively colored solutions) and with higher temperatures they grow and agglomerate to finally precipitate. When the siloxalane **6** is used instead of  $[\text{H}_2\text{AlOtBu}]$  (**3**) in solvents like toluene or THF as reductive agents, the reduction already starts at lower temperatures, since the color change is observed earlier on the temperature scale (Figure 5).

The precipitates that were obtained were isolated at room temperature and characterized by X-ray powder diffraction and revealed to be in all cases  $\beta$ -tin. In the X-ray powder diffraction diagrams of precipitates generated in polar THF, significantly broader diffraction signals appear compared to those of the powders obtained from toluene (Figure 6).

Using a modified Scherrer method it was possible to estimate an average crystallite size from the X-ray diffraction

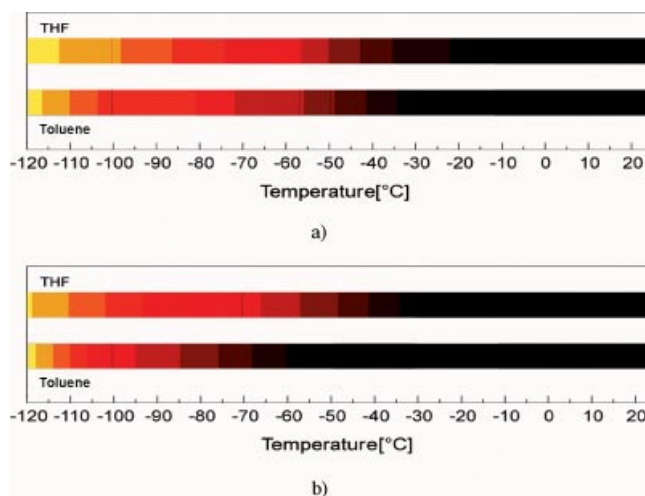


Figure 5. Colors of the reaction mixtures correlated with the temperature. Reaction of  $\text{Me}_2\text{Si}(\text{NtBu})_2\text{Sn}$  (**7**) with  $[\text{H}_2\text{AlOtBu}]$  (**3**) (a), or with  $[\text{H}_2\text{AlOSiMe}_3]$  (**6**) (b).

diagrams.<sup>[13]</sup> The results of this line analysis are shown in Table 1.

The tin particles formed by the reduction of  $[\text{Me}_2\text{Si}(\text{NtBu})_2\text{Sn}]$  (**7**) with the more reactive hydride **6** [ $\text{R} = \text{SiMe}_3$ , (b) in Table 1] show a larger average crystallite size than those formed when the hydride **3** [ $\text{R} = t\text{Bu}$ , (a) in Table 1] is used. This becomes very obvious when toluene is used as a solvent, because then the differences in the sizes are approximately 300 nm. The siloxy groups may have an influence on the most apolar solvent. On the other hand, in the more polar THF, the average crystallite sizes lie in both cases below 30 nm and using hydride **3** the crystallite size may even be below that of 20 nm. Obviously, the donor molecules like THF as well as thiophene and TMEDA in the solvent mixtures are able to stabilize the colloids in such a way that the crystallite growth is hindered. This can also be concluded from experimentally determined carbon/hydrogen contents of the precipitates generated from toluene and THF. They are, for those powders formed in THF, between 7 and 11 times higher than for those generated in toluene (Tables 2 and 3). So it is very likely that solvent molecules are coordinated on the surface of the particles. We have tried to perform HRTEM analyses on the powders, but observed high reactivities with oxygen prior to the measurements, almost excluding a proper experiment. Although we have no data for tin, we assume similar behavior as for lead.<sup>[6]</sup>

If the metal powders are allowed to interact with one another for longer times, or toluene is used as the solvent, the agglomeration continues and metal sponges are formed. In Figures 7 and 8 fragments of such a tin sponge and the corresponding SEM images are shown. The nanoscopic porosity of the sponges is clearly proved by the SEM images.

Several pycnometric measurements were carried out on the tin sponges. When water was used, an average density of  $1.5\text{ g/cm}^3$  was determined, indicating that some of the holes could not be penetrated by water. With the inert and smaller helium (which is able to fill the pores in a much

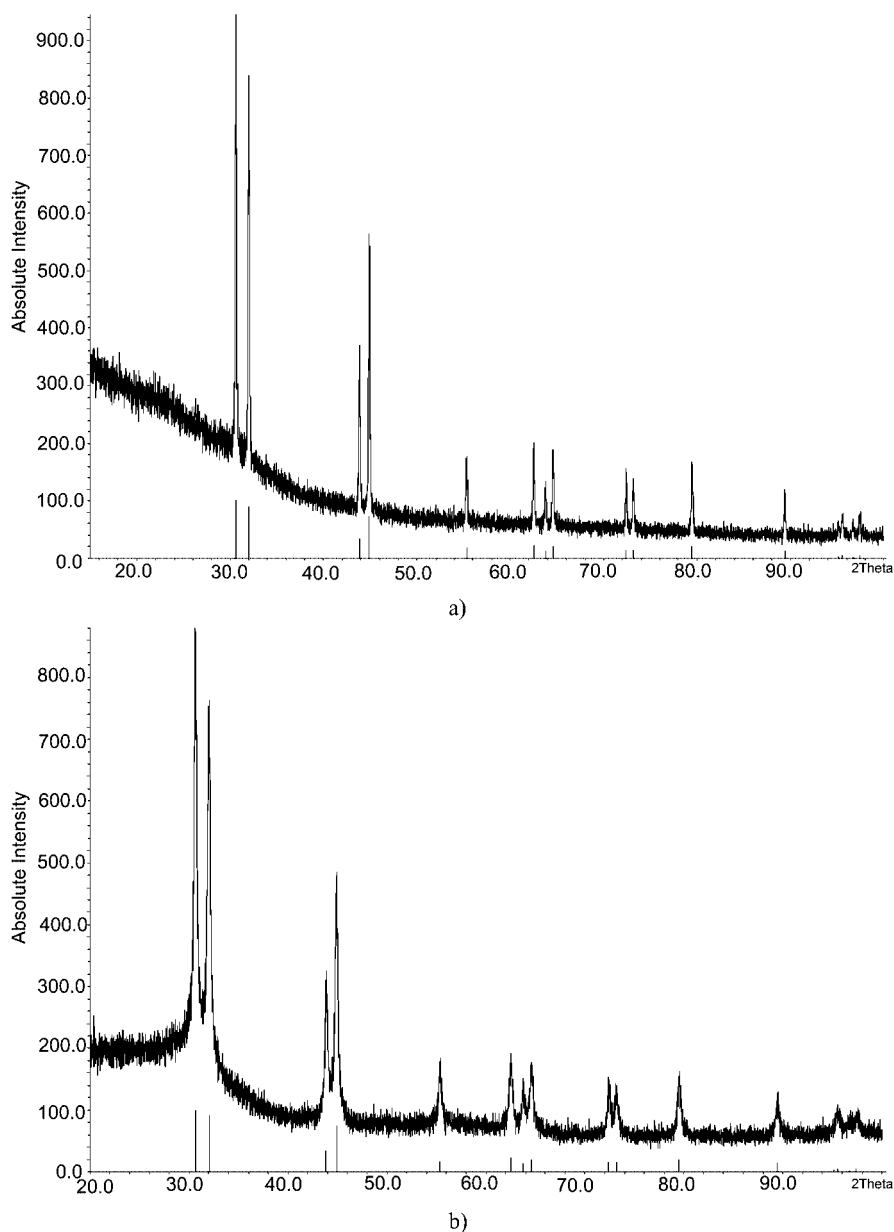


Figure 6. Powder diffraction analysis. Product from the reaction of 7 with 3 a) in toluene and b) in THF with locations of the signals and intensities of  $\beta$ -tin.<sup>[12]</sup>

Table 2. C and H contents of precipitates generated in toluene.

Reducing agent	C content	H content
[H <sub>2</sub> AlO <i>t</i> Bu] <sub>2</sub> (2)	1.47%	0.35%
[H <sub>2</sub> AlOSiMe <sub>3</sub> ] <sub><i>n</i></sub> (3)	0.83%	0.17%

Table 3. C and H contents of precipitates generated in THF.

Reducing agent	C content	H content
[H <sub>2</sub> AlO <i>t</i> Bu] <sub>2</sub> (2)	10.86%	2.45%
[H <sub>2</sub> AlOSiMe <sub>3</sub> ] <sub><i>n</i></sub> (3)	7.70%	1.91%

better way) we determined an average density of approximately 7 g/cm<sup>3</sup> for the same sponges, which is near the value of 7.3 g/cm<sup>3</sup> for pure tin.<sup>[14]</sup> For the sake of comparison we also measured the density of the corresponding lead



Figure 7. Fragments of a tin sponge. The diameters of the two bigger pieces are around 2 to 3 mm.

sponges obtained from the reactions between the lead amides and the hydrides (see ref.<sup>[6]</sup>). With water, a value of almost 8 g/cm<sup>3</sup> was obtained, and with helium the density of approximately 11 g/cm<sup>3</sup> was again close to that of lead

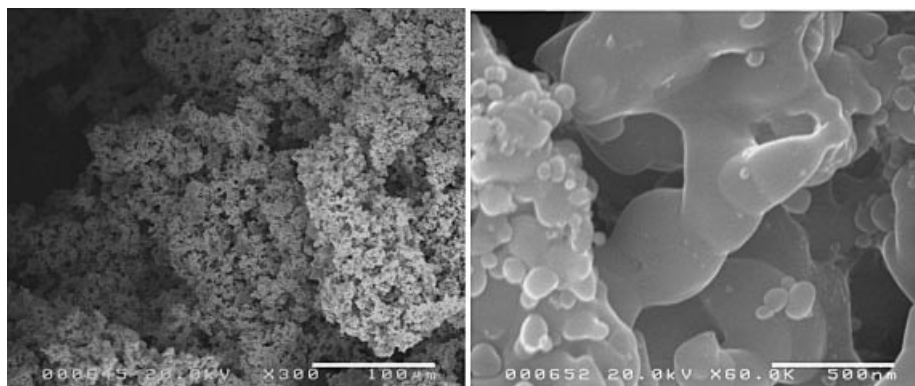


Figure 8. SEM images of a tin sponge to illustrate its high porosity. The two pictures have different scales.

(ref.<sup>[14]</sup>; 11.3 g/cm<sup>3</sup>). The mean values of the pycnometric measurements for the metal sponges in water seem to indicate a higher porosity and smaller diameters of the channels for the precipitates of tin than for those of lead.

To fill porous alumina membranes as templates with lead or tin nanoparticles we used different techniques. We have recently reported on our first attempts to fill the membranes with lead particles.<sup>[6]</sup> We managed to fill the pores up to a certain extent by treatment of the templates with colloidal solutions of different concentrations, but because of the relatively large diameters of the particles in those colloids (up to 200 nm) they covered mainly the surface of the membranes and did not fill the much smaller pores with diameters of approximately 60 nm.

For new attempts we not only used membranes with various pore diameters of 25, 30, 50, 60, 80, 90, 120 and 300 nm,<sup>[7]</sup> but also varied the filling techniques. The thickness of the membranes varied between ca. 25 μm and 90 μm and the particle sizes in the membranes are linked to the diameters of the channels as checked by XRD on selected samples after destruction. We finally succeeded in the infiltration of the membranes. Table 4 gives an overview of different possibilities to fill the membranes with tin or lead particles.

Table 4. Possibilities for membrane filling.

(i) membrane + colloidal solution	→ diffusion
(ii) membrane + colloidal solution + followed by vacuum induction of the prepared particles	
(iii) membrane + lead or tin amide solution	
	→ diffusion of the solution into the pores followed by reactions within the pores by addition of the hydride
(iv) same as in iii but with vacuum induction	

For methods (i) and (ii) the membranes were put into already prepared colloidal solutions of the metal and were filled by pure or vacuum-induced diffusion. Methods (i) and (ii) led to dark membranes because of agglomeration of the metal particles on their surfaces. These membranes were not further investigated with regard to their optical properties. For methods (iii) and (iv) the membranes were treated, after careful washing with the solvents and drying, in a first instance with the stannylene or plumbylene solutions. In a second step, they were washed with a small

amount of solvent in order to clean the surface. Finally, the metal clusters were synthesized within the membranes by reaction with the added hydrides. The channels of the membranes were filled with the amide solutions using vacuum-assisted diffusion. The routes (iii) and (iv) of Table 4 proved to be the most effective methods to fill the templates. Besides the different filling methods we also varied the concentrations of the reaction solutions, the temperature [ $<-100$  °C for (i) and (ii) and 20 °C for (iii) and (iv)] and the filling time. Finally, we repeated the filling process several times. We cannot completely exclude a side reaction of the metal amides with remaining hydroxy groups on the inner surfaces of the alumina membranes; the concentrations of the stannylene solutions were chosen in such a way that these side reactions may be almost neglected. Furthermore, we could not observe spectroscopically any of the hydrolysis byproducts of the stannylene **7**. Also the molecular byproducts described in the first section of this article have not been isolated and separated for each filling process. In the following, we want to describe in more detail mainly the filling of the membranes with tin. The experiments with lead amides showed similar results, some of which have already been documented.<sup>[6]</sup> With increasing concentrations and filling time (or repetitions of the filling process) a significant color change of the originally transparent membranes from light brown to dark brown and finally to black is observed. The infiltration can be monitored by EDX analysis. Figure 9 contains spectra of (a) a non-treated 50 nm membrane, (b) a light brown and (c) a dark brown membrane after filling with tin particles.

The signal at 3.5 keV found in the EDX spectra is characteristic for tin and a comparison of these signals with the ones of aluminum at 1.8 keV confirms a higher Sn content for the dark brown membrane. The different intensities in color of the membranes treated with differently concentrated stannylene solutions (up to 210 mmol/L) are reflected in their UV spectra shown in Figure 10. In Figure 10 (a) and (b) the spectra are shown when the hydride **3** was used for reduction, whereas Figures 10 (c) and (d) contain the spectra for when the hydride **6** was used (the self absorption of the membrane is subtracted in the spectra on the right-hand side). With increasing concentrations of stannylene and longer filling times the maxima of the absorptions be-

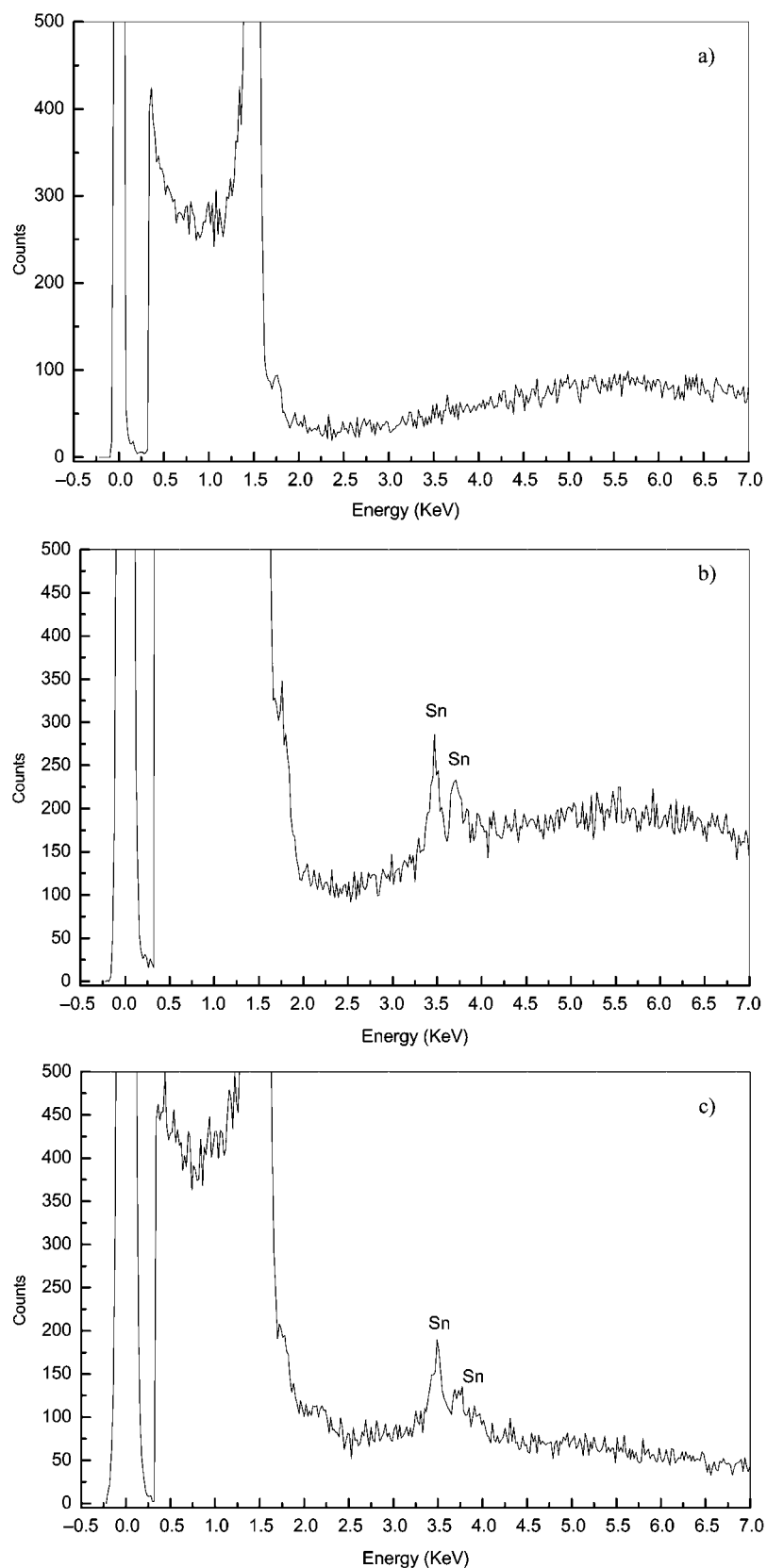
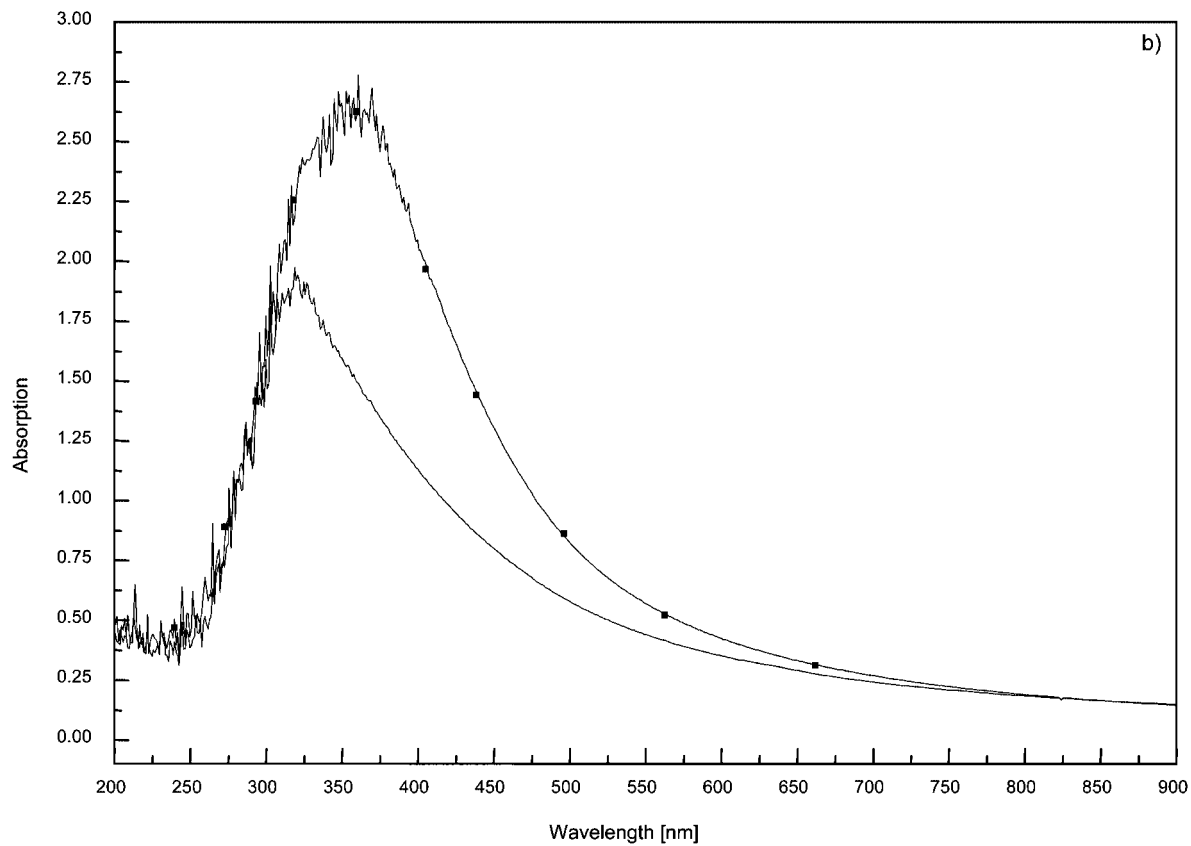
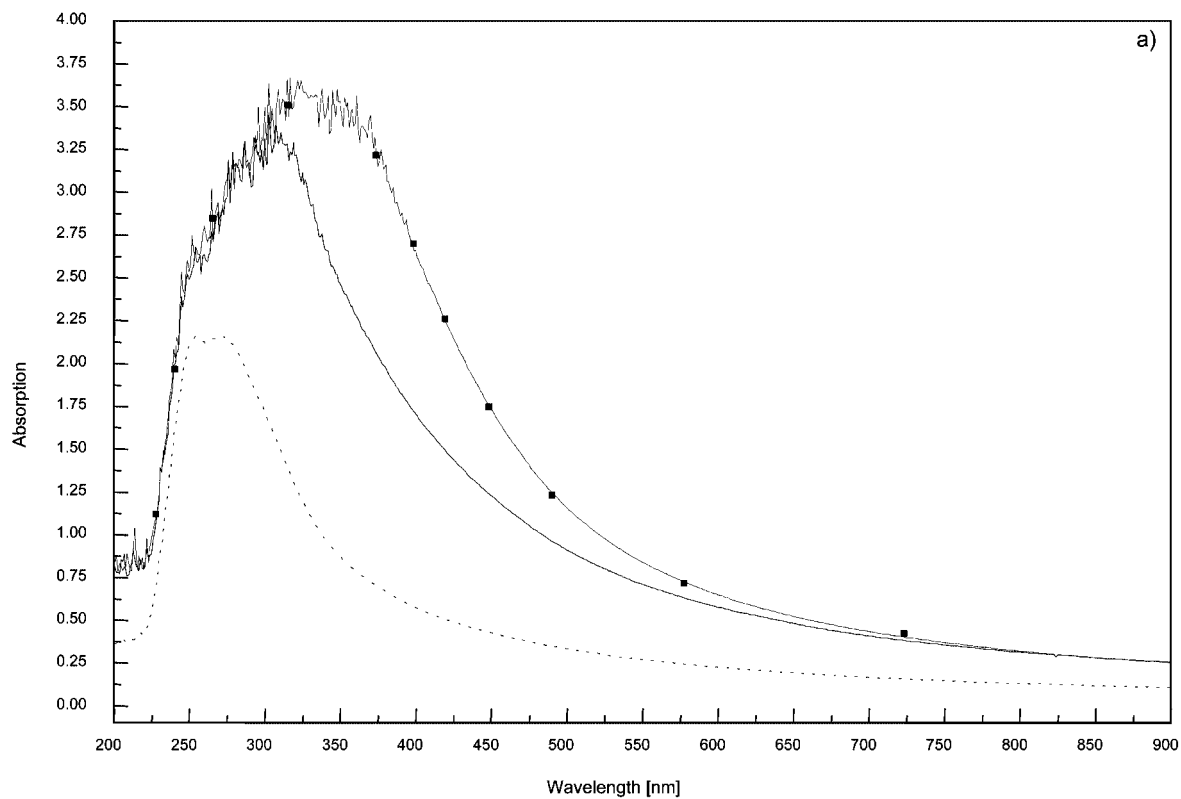


Figure 9. EDX spectra of (a) a nontreated 50 nm membrane, (b) a light brown and (c) a dark brown membrane after filling with tin particles. Experimental conditions: concentration of 7.137 mmol/L or 411 mmol/L in THF, hydride **3**, method (iv) of Table 4, vacuum induction time 5 min each.



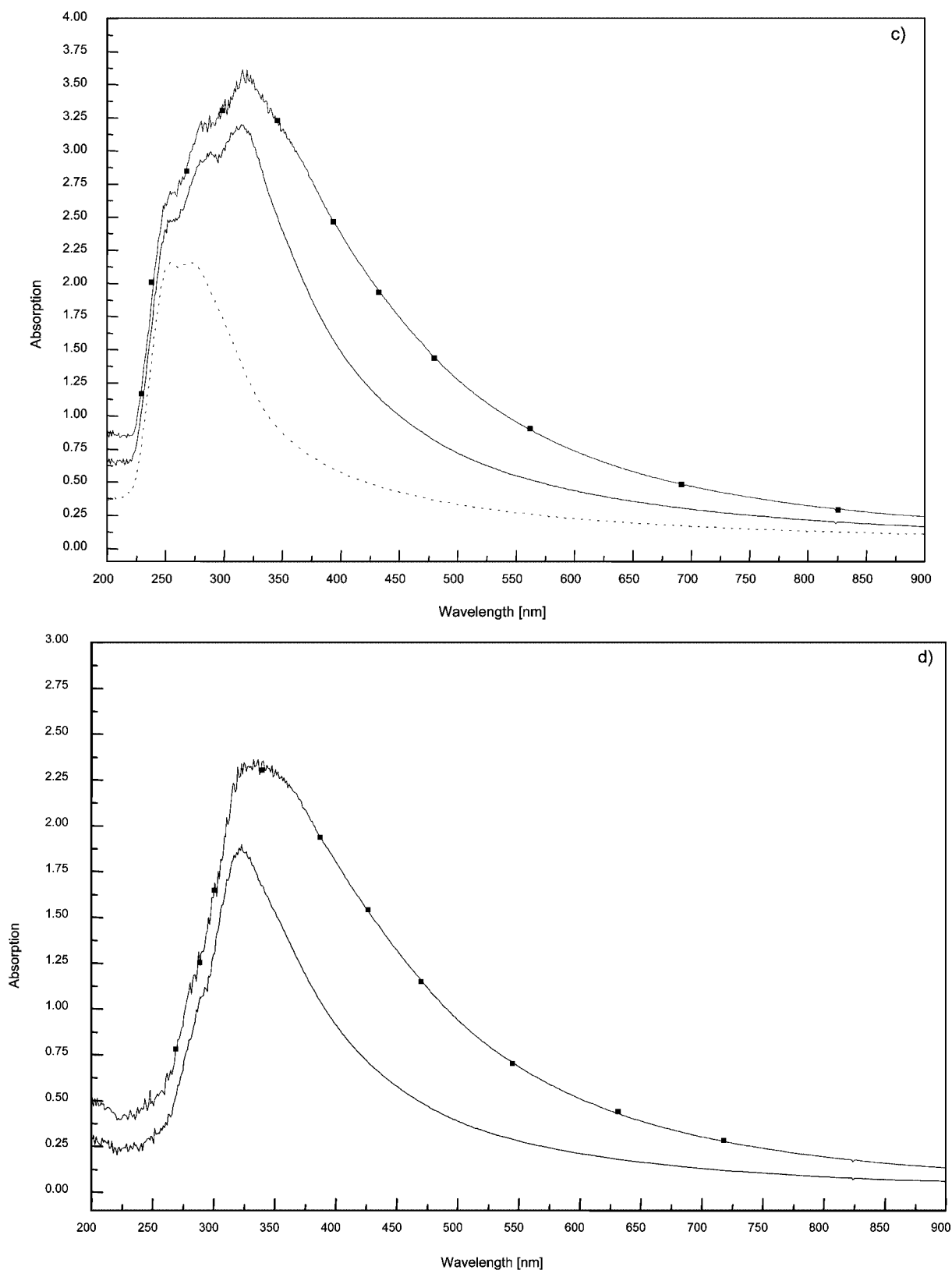


Figure 10. UV spectrum of a 50 nm membrane with respect to the concentration of stannylene **7** and the time of vacuum induction. The reductive agent for (a) and (b) is hydride **3** ( $c_{\text{stannylene}} = 137$  mmol/L, 5 min vacuum induction;  $\blacksquare$   $c_{\text{stannylene}} = 210$  mmol/L, 5 min vacuum induction;  $\cdots$  absorption of the membrane), for (c) and (d), hydride **6** ( $c_{\text{stannylene}} = 121$  mmol/L, 5 min vacuum induction;  $\blacksquare$   $c_{\text{stannylene}} = 200$  mmol/L, 10 min vacuum induction;  $\cdots$  absorption of the membrane). On the right-hand side the absorption of the membrane is subtracted.

come more intense and the bands are widened due to the bigger sizes and the larger amounts of particles. In addition, the absorption maxima are shifted towards higher wavelengths when the amount of aggregating tin clusters increases leading to an interaction of their plasmon resonances (see also ref.<sup>[6]</sup> for further discussion).

Already from a visual comparison it becomes evident that the different reactivities of the reductive agents **3** and **6** has only little influence on the color of the treated membranes as shown by their UV spectra. All filled membranes show almost identical absorption curves depending on the concentration of tin clusters.

Dark brown or black membranes result from very high concentrations of stannylene (>350 mmol/L). The absorption spectra show broad signals with very high intensities. Such a spectrum is presented in Figure 11 (concentration of stannylene **7**: 360 mmol/L; reductive agent hydride **3**). It shows an impervious range between 270 and 500 nm. Such

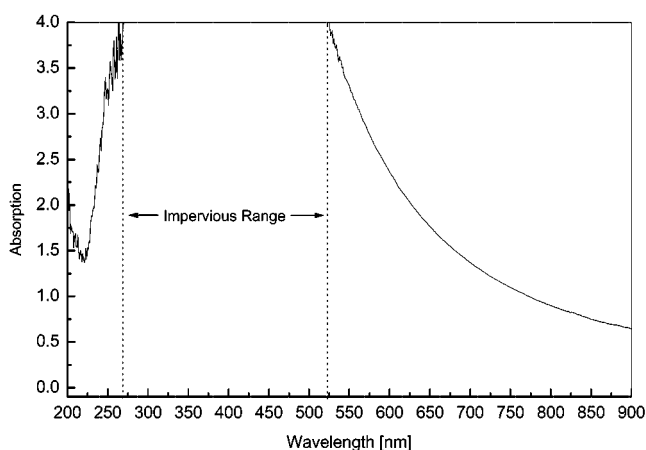


Figure 11. UV/Vis absorption spectrum of a very colored membrane; concentration of stannylene **7**: 360 mmol/L; reductive agent hydride **3**.

a membrane could be used as a wavelength filter, which absorbs the light completely within a well-defined range. The transmission spectrum shown in Figure 12 (concentration of stannylene **7**: 411 mmol/L; reductive agent hydride **6**) underlines this possibility for use. Here one finds an impervious range between 250 and 525 nm.

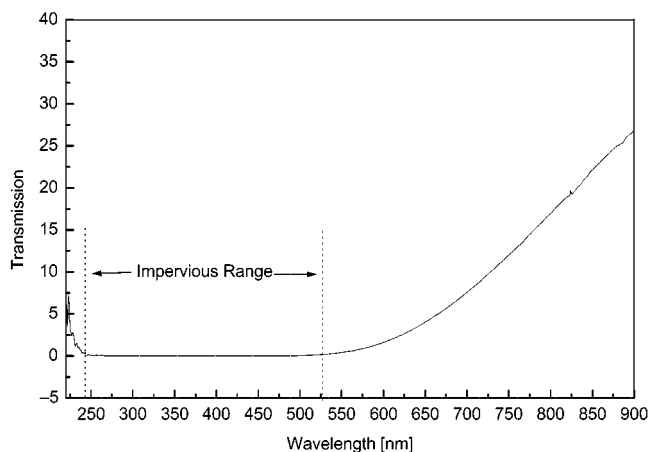


Figure 12. UV/Vis transmission spectrum of a very colored membrane; concentration of stannylene **7**: 411 mmol/L; reductive agent hydride **6**.

As mentioned above, we have used membranes with different pore diameters and the UV spectra of these membranes (filled under similar conditions) show a shift of the absorption maxima towards higher wavelengths (Figure 13). Obviously, the size of the metal clusters plays an important role.<sup>[6]</sup> As the absorption maxima shift with the pore diameter (with parallel increase of the metal particle diameters) one may use the process to produce wavelength filters of different absorption maxima.

We noticed an improvement in the infiltration of the membranes when we repeated the filling process several times. As expected, the filling of the channels is most effec-

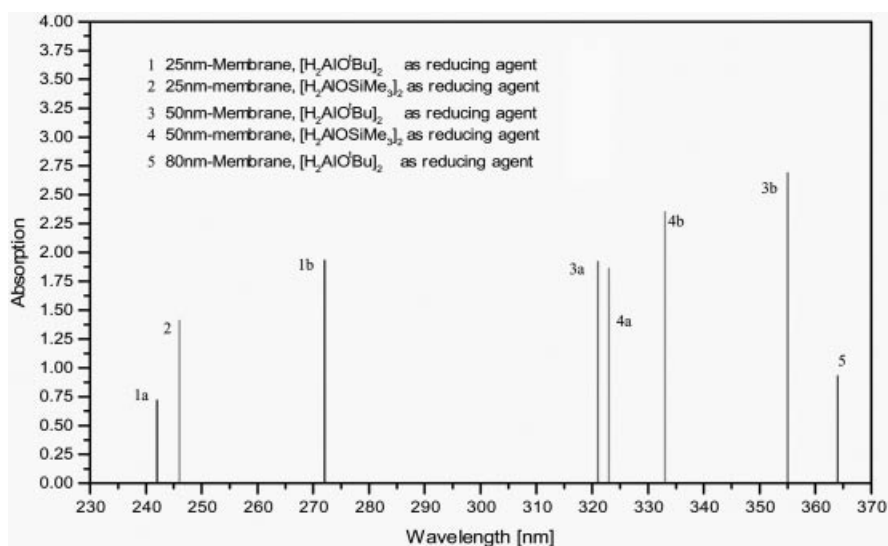


Figure 13. Comparison of the position of the absorption maxima using membranes of different pore diameters filled with tin particles (a and b stand for different probes of the same material).

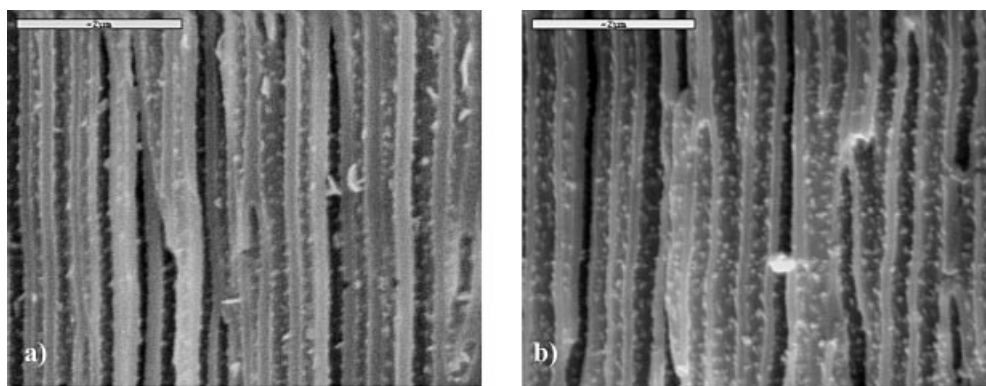


Figure 14. SEM images of (a) 5 and (b) 10 times filled 300 nm Al<sub>2</sub>O<sub>3</sub> membranes to show the increase in the amount of lead particles within the pores (ca. 10 kV sputtered with approximately 10 nm Au).

tive for membranes with large pore diameters. The SEM images of a 300 nm Al<sub>2</sub>O<sub>3</sub> membrane filled with lead particles after five and ten infiltrations are presented in Figure 14. They show an increase in the amount of lead clusters with repetitive filling. The repetition is nevertheless limited due to a blocking of the pores after ca. 7–8 cycles. The particles in the 300 nm pores have mean diameters of 80–90 nm.

## Summary and Conclusion

Tin and lead nanosized particles and metal sponges have been prepared by reduction of molecular tin(II) and lead(II) amides with siloxy- and alkoxyalanes in non-aqueous media. The resulting molecular byproducts have been isolated and (structurally) characterized. Colloidal solutions of tin were obtained when the reaction mixture was slowly warmed from –115 °C to room temperature. With agglomeration of the particles in this solution, tin powders formed and precipitated, and have been identified as β-tin by EDX analysis. Their average particle size diameter can be controlled either by using different donor solvents or different hydrides as reducing agents. The smallest particles were obtained when *tert*-butoxyalane **3** was used as hydride and THF as donor solvent. The metal sponges were characterized by pycnometric measurements with helium and water and show a lower density compared with their value known from literature when water was used because of its surface tension and the high porosity of the metal precipitates. Porous aluminum oxide membranes with different pore diameters were used as templates for ordering tin or lead clusters within the pores. The metal particles were prepared by reduction of the metal amides within the membranes and the amount of particles could be increased by repetition of the filling process, which was an improvement in the infiltration compared to our former attempts. Differently colored membranes resulted from the filling process and were characterized by UV/Vis spectroscopy. Depending on the concentration of the starting materials and the pore diameters of the membranes they showed impervious ranges, which enabled these membranes to be used as wavelength filters.

## Experimental Section

**Physical Measurements:** The elemental analyses of the compounds were carried out using a CHN analyzer from LECO™ Corporation, St. Joseph, MI, U.S.A. The NMR spectra were measured with Bruker 200 MHz spectrometers, model AC 200 F (<sup>1</sup>H and <sup>13</sup>C spectra) and AC 200 P (<sup>29</sup>Si spectra), using [D<sub>6</sub>]benzene as solvent. The single-crystal X-ray analyses were performed either with an Image Plate (IPDS I), or a four-circle diffractometer (STADI 4) (Stoe, Dramstadt). The structure calculations were carried out with SHELXS97<sup>[15]</sup> and the graphical representation with Diamond 3.<sup>[16]</sup> The complete crystal structure data are deposited with the Cambridge Crystallographic Data Centre (CCDC), 12 Union Road, Cambridge CB2 1 EZ (UK) [CCDC-270194 (**10**), 270195 (**11**), and 270196 (**12**)]. The powder diffraction measurements of the tin and lead precipitates were performed in a glass capillary with a Stoe diffractometer, model STADIP, using Cu-K<sub>α</sub> radiation with a wavelength of 1.540598 Å and a linear PSD detector. The measurements were analyzed with the software WinX<sup>Pow</sup>. The electron microscopy (SEM) and energy-dispersive X-ray analyses (EDX) were performed with a scanning electron microscope CAM-SCAN S4 with Si(Li) semiconductor detectors and with thin windows (Cameca and Noran). To perform the SEM analyses of the filled membranes, the membranes were covered with gold. The UV/Vis spectra were measured with a Perkin–Elmer spectrometer, model Lambda 35.

**Synthetic Procedures:** All compounds were synthesized under dry nitrogen using standard Schlenk techniques. The solvents were dried by refluxing with appropriate drying agents and distilled before being used.

**[Me<sub>2</sub>(N*t*Bu)<sub>2</sub>Al(O*t*Bu)(THF)] (**11**):** Me<sub>2</sub>Si(N*t*Bu)<sub>2</sub>Pb (**9**) (2.82 g, 6.92 mmol) in THF (25.0 mL) was added dropwise to a stirred solution of [H<sub>2</sub>AlO*t*Bu]<sub>2</sub> (**3**) (0.71 g, 3.46 mmol) in dry THF (25.0 mL) and allowed to react at room temperature for 24 h. The reaction mixture turned grey, the lead precipitated and gas (hydrogen) evolved. When the reaction was complete, the solution was separated from the lead and concentrated until crystals of [Me<sub>2</sub>(N*t*Bu)<sub>2</sub>Al(O*t*Bu)(THF)] (**11**) formed. After recrystallization of the crude product from THF, **11** (1.48 g, 3.97 mmol) may be obtained, at 4 °C, as colorless crystals (yield: 57%). Molecular mass: 372.60 g/mol. <sup>1</sup>H NMR (200 MHz, C<sub>6</sub>D<sub>6</sub>, 25 °C): δ = 0.45 [s, 3 H, Si(CH<sub>3</sub>)<sub>2</sub>], 0.57 [s, 3 H, Si(CH<sub>3</sub>)<sub>2</sub>], 1.09 (m, 4 H, THF), 1.37 (s, 18 H, N*t*Bu), 1.51 (s, 9 H, O*t*Bu), 3.82 (m, 4 H, THF) ppm. <sup>13</sup>C NMR (200 MHz, C<sub>6</sub>D<sub>6</sub>, 25 °C): δ = 7.09 [s, 1 C, Si(CH<sub>3</sub>)<sub>2</sub>], 7.27 [s, 1 C, Si(CH<sub>3</sub>)<sub>2</sub>], 24.81 (s, 2 C, THF), 34.12 (s, 3 C, O*t*Bu), 36.45 (s, 6 C, N*t*Bu), 49.50 (s, 2 C, quat. C, N*t*Bu), 71.03 (s, 2 C, THF),

78.16 (s, 1 C, quat. C, *Or*Bu) ppm.  $^{29}\text{Si}$  NMR (200 MHz,  $\text{C}_6\text{D}_6$ , 25 °C):  $\delta = -15.55$  [s, 1 Si,  $\text{Si}(\text{CH}_3)_2$ ] ppm. Compound **11** crystallizes in the monoclinic space group *I2/a* with  $Z = 8$  [ $a = 15.724(3)$ ,  $b = 15.529(3)$ ,  $c = 19.917(4)$  Å,  $\beta = 92.97(3)^\circ$ ,  $V = 4856.8(16)$  Å<sup>3</sup>],  $1.84^\circ < \theta < 23.92^\circ$ , 14862 reflections collected, 3738 unique ( $R_{\text{int}} = 0.1329$ ), the structure was solved by direct methods and refined by full-matrix least squares on  $F^2$ . Final  $R_1 = 0.0555$  ( $I > 2\sigma_I$ ) and  $wR_2 = 0.1331$  with an electron density left of  $0.409/-0.279$  e/Å<sup>3</sup>.

**[Me<sub>2</sub>Si(N*t*Bu)<sub>2</sub>Al(OSiMe<sub>2</sub>*t*Bu)(THF)] (10):** Analogous to the synthesis of compound **11** (at room temperature). Yield: 63%. Molecular mass: 430.76 g/mol, calcd. C 55.77, H 11.0, Al 6.26, N 6.5; found C 55.18, H 10.78, Al 6.62, N 6.57.  $^1\text{H}$  NMR (200 MHz,  $\text{C}_6\text{D}_6$ , 25 °C):  $\delta = 0.28$  [s, 6 H, OSi(CH<sub>3</sub>)<sub>2</sub>], 0.44 [s, 3 H, Si(CH<sub>3</sub>)<sub>2</sub>], 0.57 [s, 3 H, Si(CH<sub>3</sub>)<sub>2</sub>], 1.08 (m, 4 H, THF), 1.14 (s, 9 H, *Sit*Bu), 1.34 (s, 18 H, *Nt*Bu), 3.8 (m, 4 H, THF) ppm.  $^{13}\text{C}$  NMR (200 MHz,  $\text{C}_6\text{D}_6$ , 25 °C):  $\delta = -1.91$  [s, 2 C, OSi(CH<sub>3</sub>)<sub>2</sub>], 6.36 [s, 1 C, Si(CH<sub>3</sub>)<sub>2</sub>], 6.7 [s, 1 C, Si(CH<sub>3</sub>)<sub>2</sub>], 18.39 (s, 1 C, quat. C, *Sit*Bu), 24.33 (s, 2 C, THF), 26.26 (s, 3 C, *Sit*Bu), 35.89 (s, 6 C, *Nt*Bu), 48.85 (s, 2 C, quat. C, *Nt*Bu), 70.74 (s, 2 C, THF) ppm.  $^{29}\text{Si}$  NMR (200 MHz,  $\text{C}_6\text{D}_6$ , 25 °C):  $\delta = -14.98$  [s, 1 Si, Si(CH<sub>3</sub>)<sub>2</sub>], 4.8 (s, 1 Si, OSi) ppm. Compound **10** crystallizes in the monoclinic space group *P2<sub>1</sub>/c* with  $Z = 4$  [ $a = 12.095(2)$ ,  $b = 10.637(2)$ ,  $c = 21.629(4)$  Å,  $\beta = 97.67(3)^\circ$ ,  $V = 2757.8(9)$  Å<sup>3</sup>],  $1.90^\circ < \theta < 23.99^\circ$ , 16615 reflections collected, 4214 unique ( $R_{\text{int}} = 0.1215$ ), the structure was solved by direct methods and refined by full-matrix least squares on  $F^2$ . Final  $R_1 = 0.0546$  ( $I > 2\sigma_I$ ) and  $wR_2 = 0.1393$  with an electron density left of  $0.358/-0.287$  e/Å<sup>3</sup>.

**[Me<sub>2</sub>Si(N*t*Bu)<sub>2</sub>Al(OSiMe<sub>2</sub>*t*Bu)]<sub>2</sub> (12):** Compound **12** can be synthesized in the same manner as compound **10**, but by heating the reaction mixture under reflux. Yield: 81%. Molecular mass: 789.83 g/mol, calcd. C 48.69, H 9.96, Al 6.84, N 7.1; found C 48.16, H 9.76, Al 6.91, N 6.83.  $^1\text{H}$  NMR (200 MHz,  $\text{C}_6\text{D}_6$ , 25 °C):  $\delta = 0.51$  [s, 18 H, OSi(CH<sub>3</sub>)<sub>2</sub>], 0.61 [s, 12 H, Si(CH<sub>3</sub>)<sub>2</sub>], 1.12 (s, 18 H, *Sit*Bu), 1.38 (s, 36 H, *Nt*Bu) ppm.  $^{13}\text{C}$  NMR (200 MHz,  $\text{C}_6\text{D}_6$ , 25 °C):  $\delta = -0.41$  [s, 4 C, OSi(CH<sub>3</sub>)<sub>2</sub>], 7.27 [s, 4 C, Si(CH<sub>3</sub>)<sub>2</sub>], 19.49 (s, 2 C, quat. C, *Sit*Bu), 27.06 (s, 6 C, *Sit*Bu), 36.27 (s, 12 C, *Nt*Bu), 49.62 (s, 4 C, quat. C, *Nt*Bu) ppm.  $^{29}\text{Si}$  NMR (200 MHz,  $\text{C}_6\text{D}_6$ , 25 °C):  $\delta = -9.39$  [s, 2 Si, Si(CH<sub>3</sub>)<sub>2</sub>], 29.46 (s, 2 Si, OSi) ppm. Compound **12** crystallizes in the monoclinic space group *P2<sub>1</sub>/n* with  $Z = 8$  [ $a = 27.779(6)$ ,  $b = 11.612(2)$ ,  $c = 28.043(6)$  Å,  $\beta = 97.89(3)^\circ$ ,  $V = 8960(3)$  Å<sup>3</sup>],  $1.90^\circ < \theta < 24.05^\circ$ , 55081 reflections collected, 13935 unique ( $R_{\text{int}} = 0.0897$ ), the structure was solved by direct methods and refined by full-matrix least-squares on  $F^2$ . Final  $R_1 = 0.0904$  ( $I > 2\sigma_I$ ) and  $wR_2 = 0.2245$  with electron density left:  $2.689/-1.741$  e/Å<sup>3</sup>.

## Acknowledgments

Authors thank the "Deutsche Forschungsgemeinschaft (DFG)" for providing financial support in the framework of the research program "Halbleiter und Metallcluster als Bausteine für organisierte Strukturen" (SPP 1072) as well as Prof. Dr. G. Schmid, Essen, for providing the membranes. Dr. M. Ehse, Saarbrücken, is acknowledged for kindly reading the manuscript.

[1] U. Kreibitz, M. Vollmer, *Optical Properties of Metal Clusters*, Springer, New York 1995.

- [2] G. Schmid (Ed.), *Clusters and Colloids*, VCH, Weinheim, 1994.
- [3] a) G. Schmid, *Nach. Chem. Tech. Lab.* **1987**, *35*, 249; b) G. Schmid, *Chem. Unserer Zeit* **1988**, *22*, 85; c) G. Schmid, B. Morun, J.-O. Malm, *Angew. Chem.* **1989**, *101*, 772; d) G. Schmid, A. Lehnert, U. Kreibitz, Z. Adamczyk, P. Belouschek, *Z. Naturforsch., Teil B* **1990**, *45*, 989–994; e) G. Schmid, R. Küpper, H. Hess, J.-O. Malm, J.-O. Bovin, *Chem. Ber.* **1991**, *124*, 1889–1893; f) G. Schmid, M. Harms, J.-O. Malm, J.-O. Bovin, J. Van Ruitenbeck, H. W. Zandbergen, W. T. Fu, *J. Am. Chem. Soc.* **1993**, *115*, 2046–2048; g) U. Simon, G. Schön, G. Schmid, *Angew. Chem.* **1993**, *105*, 264–267; h) J. G. A. Dubois, J. W. Gerritsen, G. Schmid, H. van Kempen, *Physica B* **1995**, *204*, 51–56; i) S. Peschel, G. Schmid, *Angew. Chem.* **1995**, *107*, 1568–1569; j) J. G. A. Dubois, J. W. Gerritsen, G. Schmid, H. van Kempen, *Physica B* **1996**, *218*, 262; k) A. Bezryadin, C. Dekker, G. Schmid, *Appl. Phys. Lett.* **1997**, *71*, 1273–1275; l) G. Schmid, St. Peschel, T. Sawitowski, *Z. Anorg. Allg. Chem.* **1997**, *623*, 719–723; m) G. Schmid, *J. Chem. Soc., Dalton Trans.* **1998**, 1077–1082; n) G. Schmid, N. Beyer, *Eur. J. Inorg. Chem.* **2000**, 835–837.
- [4] a) C. Nayral, T. Ould-Ely, A. Maisonnat, B. Chaudret, P. Fau, L. Lescouzères, A. Peyre-Lavigne, *Adv. Mater.* **1999**, *11*, 61–63; b) C. Nayral, E. Viala, P. Fau, F. Senocq, J. C. Jumas, A. Maisonnat, B. Chaudret, *Chem. Eur. J.* **2000**, *6*, 4082; c) G. Cardenas-Trivino, M. Alvial, K. J. Klabunde, O. Pantoja, H. Soto, *Colloid Polym. Sci.* **1994**, *272*, 310–316; d) P. Cheyssac, M. Geddo, R. Kofman, P. G. Merli, A. Migliori, A. Stella, P. Tognini, *Mater. Sci. Forum* **1995**, *195*, 161; e) B. Ocker, R. Wurster, H. Seiler, *Scanning Microsc.* **1995**, *9*, 63; f) A. Henglein, M. Giersig, *J. Phys. Chem.* **1994**, *98*, 6931–6935; g) G. Sberveglieri, *Sens. Actuators B* **1992**, *6*, 239.
- [5] M. Veith, O. Schütt, J. Blin, J. Frères, S. Becker, V. Huch, *Z. Anorg. Allg. Chem.* **2001**, *628*, 138–146.
- [6] M. Veith, S. Mathur, P. König, C. Cavelius, J. Biegler, A. Rammo, V. Huch, H. Shen, G. Schmid, *C. R. Chim.* **2004**, *7*, 509–519.
- [7] a) G. Hornyak, M. Kröll, R. Pugin, T. Sawitowski, G. Schmid, J.-O. Bovin, G. Karsson, H. Hofmeister, S. Hopfe, *Chem. Eur. J.* **1997**, *3*, 1951–1956; b) G. Schmid, L. F. Chi, *Adv. Mater.* **1998**, *10*, 515; c) T. Hanaoka, H.-P. Kormann, M. Kröll, T. Sawitowsky, G. Schmid, *Eur. J. Inorg. Chem.* **1998**, 807; d) P. Braunstein, H. P. Kormann, W. Meyer-Zaika, R. Pugin, G. Schmid, *Chem. Eur. J.* **2000**, *6*, 4637–4646.
- [8] M. Veith, M. Grosser, *Z. Naturforsch. B. Anorg. Chem.* **1982**, *37*, 1375–1381.
- [9] M. Veith, S. Faber, H. Wolfanger, V. Huch, *Chem. Ber.* **1996**, *129*, 381.
- [10] J. Blin, Dissertation, Universität des Saarlandes 1999.
- [11] M. Veith, *Angew. Chem.* **1975**, *87*, 278; *Angew. Chem. Int. Ed. Engl.* **1975**, *14*, 263.
- [12] JCPDS-Datei, [4-673], from ICDD database.
- [13] Steuerungssoftware des STOE-Transmissions-Diffraktometers STADIP: WINXPOW Version 1.03, 1998, and STOE VISUALXP.
- [14] A. F. Holleman, E. Wiberg, N. Wiberg, *Lehrbuch der anorganischen Chemie*, 2nd ed., Walter de Gruyter, Berlin, New York, 1995.
- [15] G. Sheldrick, *Program for Crystal Structure Solution*, version SHELX-97, Göttingen, 1997.
- [16] M. Berndt, K. Brandenburg, H. Putz, *Visual Crystal Structure Information System*, Diamond version 3, Bonn, 1996–2005.

Received: April 26, 2005

Published Online: August 30, 2005